Fabrication and Mechanical Testing of Mesoscale Specimens

ARIJIT LODH [iD],[1,3] CLEMENT KELLER,[2,4]
and GUSTAVO M. CASTELLUCCIO[1,5]

1.—School of Aerospace, Transport and Manufacturing, Cranfield University, Bedfordshire MK43 0AL, UK. 2.—Laboratoire Génie de Production, ENIT-INP, Avenue d'Azereix, 65000 Tarbes, France. 3.—e-mail: a.lodh@cranfield.ac.uk. 4.—e-mail: ckeller@enit.fr. 5.—e-mail: castellg@cranfield.ac.uk

The mechanical response of metallic materials results from a complex hierarchy of deformation mechanisms across length scales. The need to understand these mechanisms independently has driven the miniaturization of testing samples, including small scale samples and single crystal micropillars. However, difficulties in machining and testing small samples have hampered the evaluation of the mechanical response of mesoscale samples with dimensions between tens to hundreds of microns. This paper innovates with a simple approach for the manufacturing and test of dog-bone specimens with a minimum gauge width up to 50 μm. The results demonstrate a pronounced sample size effects on the mechanical response for the dimensions analysed and highlights the need to advance the characterization of mesoscale samples. We also demonstrated the capability of testing the tensile response of single crystals from engineering alloys.

INTRODUCTION

The mechanical response of metallic materials arises from different deformation mechanisms that coexist across several length scales. Concurrent interactions among these mechanisms make it difficult to characterize them independently and requires multiscale experimental and modeling approaches. Crystal plasticity simulations[1,2] have demonstrated the need of single crystal data to correctly parameterize physics-based multiscale models.

Recent research efforts have recently focused on small-scale testing to assess microstructure–property relationships of single- and poly-crystals.[3–5] Unlike standardized approaches that are available for dimensions up to a few millimetre (e.g., ASTM standard),[6] no standards are available specifically for mechanical testing of submillimetre specimens. Researchers have advanced the miniaturization of mechanical testing by developing millimetre-size

samples[7] machined from scarce material sources such as irradiated,[8–10] hydrogen embrittled,[11] or welded components.[12,13]

One of the challenges of miniaturization is the need for accurate machining and transference into a different testing device. Researchers have explored micron-scale sample testing by employing nanoindentation,[14,15] micro-tensile stages,[8,16,17] and micro-compressive testing,[18–20] micro-cantilever testing[21] under in-situ conditions. These techniques are naturally better suited for cutting and testing volumes of a few microns in a single testing machine. Hence, they rapidly become impractical for samples of several tens of microns or more. At these length scales, the mechanical properties of metals are relatively unexplored despite being relevant to a range of macroscopic properties (e.g., microstructure, dislocation substructures).

In the last two decades, increasing demand of micro-engineering components has improved micromachining process, which made miniaturization of metallic, ceramic and polymeric components possible. Appropriate controlling units have enabled nano-scale precisions with a number of micromachining methods.[22–24] A relatively common approach to fabricate micron-sized specimens employs Focused Ion Beam (FIB) milling (e.g.,

Ga$^+$, Xe$^+$ etc).[3,25,26] Small ion sources reduce the spot size[27] and allow for ultra-small designs, but they typically have low removal rate ($\sim$20 μm^{3}s^{-1}), which makes the process expensive and impractical. In addition, FIB can result in surfaces contamination and damage that leads to pseudo-surface hardening, grain size or texture change.[28,29]

Other approaches such as Microelectrical Discharge Machining (μ-EDM),[30,31] laser beam micromachining[32–34] or TriBeam systems (femtosecond laser and FIB combined in SEMs)[35,36] have been used sucessfully. However, equipment high cost, implantation damage, and variability in material properties (conductivity, reflectivity) hinder their universal generalization.

More traditional mechanical machining approaches have been miniaturized successfully and at relatively lower costs. For example, abrasive waterjet (AWJ),[24] polishing-grinding,[37–39] electrochemical machining,[40] have produced small-scale samples. Probably the most accurate machining approach corresponds to cutting methods such as microturning, microdrilling, micromilling, and micro grinding. In particular, computerized numerically controlled (CNC) vertical machining systems[41] can result in high precision specimens at a more economic cost and flexibility for a wide range of materials.

Following sample preparation, there are numerous challenges in testing the mechanical response. As the specimen size goes down, conventional mechanical testing equipments lack the resolution (mainly in displacements), making them unsuitable for testing. Much literature has used micronscale samples with piezo-actuated loading set-ups or in-situ micro/nano indentation set-ups to deform micron-scale samples. These systems can measure displacement more accurately using in-situ configurations, but they often present limitations in the loading capabilities (e.g., only monotonic loads, lack of fully reversed loading, unavailability of standard grips etc).

A major concern when testing small samples is the measurement of strain, as conventional gauges or clips cannot be fitted to the specimens. Instead, experiments have relied on non-contact strain measurements such as digital image correlation (DIC), differential digital image tracking (DDIT), interferometric strain displacement gauge etc. DIC and DDIT have the advantage of quantifying strain fields but they require sharp images with distinctive patterns.

This paper presents a miniaturization approach and demonstrates a simple and robust method to manufacture and test dog-bone specimens with gauge widths ranging from 50 μm to 500 μm (mesoscale samples). We developed a high-precision manufacturing route using micromilling to produce single- and poly-crystalline samples, which were tested in a regular screw-controlled mechanical testing machine. The results demonstrate that the technique can characterize size effects in single crystal from engineering alloys.

MESOSCALE SAMPLE

Fabrication Protocol

Given the flexibility to machine most materials at lower costs, we developed a CNC micromilling protocol to produce mesoscale tensile samples shown in Fig. 1. This specimen has a width to length ratio of 4:1, which follows the standardized design in ASTM E8/E8M.[6] Since the width of the grip section is very large compared to the gauge width, double notches were added for the safety of sample during handling.

The manufacturing process begins by cutting as-produced metals into sheets using slow-speed cutter followed by polishing. Specimen fabrication continued using a KERN EVO Micromilling unit with positioning accuracy and resolution of 1 μm and 0.1 μm, respectively. The tool has a 3/5 axis micromilling and drilling unit, equipped with cutting tool setting, auto tool change. A camera positions the tool and monitors the sample removal process while a probing tool limits the cutting dimensions. All micromachining steps employ dry machining.

A two-step procedure was followed for specimen preparation. First, coupons (12 mm $\times$ 2 mm $\times$ 0.4 mm) were cut using a 1.5 mm diameter coated flute type cutting tool (CSS 2015 - 0300 UT COAT) with a flute length of 3 mm. This tool is capable of machining copper as well as high hardness steel. With a new groove shape of the cutting tool, cutting chip discharge properties are improved and new coating has provided significant improvements in terms of fracture and wear resistance. The burrs generated after the cutting coupons were removed by polishing the coupons with a 2000 grit abrasive paper only from the sample surface. The edges of the specimens were not subjected to any polishing to avoid any distortion due to handling.

Next, the coupons were fixed in a custom-made sample holder (Fig. 2a) to constraint movement during the metal removal process. The fixture has a rectangular slot with same dimension of the coupon and was clamped with a 0.5 mm thick brass plate with a 5 mm $\times$ 10 mm slot. The centers of the slot and coupon coincide, keeping the middle area of
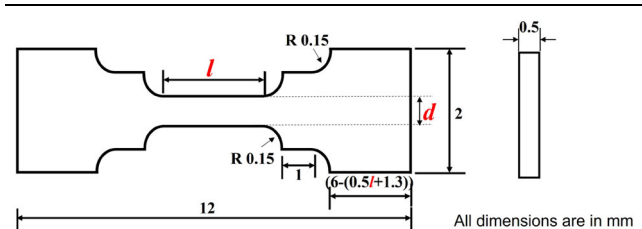

Fig. 1. Illustration of the miniaturized specimen geometry employed in this study. *l* and *d* are gauge length and width respectively. (image not in scale, all dimensions are in mm) (Color figure online).

coupon open for machining. The complete assembly was then placed inside the KERN EVO unit and the probing tool was used to find the centre of the slot. A 0.3 mm diameter carbide cutting tool having a flute length of 0.6 mm (C-CHES 2003 - 0060) was then used to machine the specimen of desired dimensions. This square-type end mill is also capable to machine wide range of materials (up to 55 HRC) and gives high quality finishing at a cost effective price.

A computerised routine machines the dog-bone shape in four steps as shown in Fig. 2b. The input program controls the lengths of the cuts to the desired sample dimensions. Table I presents the cutting parameters, which were adjusted to minimize burrs and improve surface quality. Similar to the coupons, the burrs after the sample preparation were removed with a 4000 grit abrasive paper. On an average, the preparation of a specimen takes less than one hour.

The fabrication route successfully produced specimens with gauge widths from 50 μm to 1 mm and specimen thickness from 400 to 500 μm. Given that smaller samples can withstand lower cutting forces from the endmills to avoid buckling and failure of specimens, we limited the gauge width and

Front view   **Top view**

(a)

Starting position of cutting tool

After 1st pass   After 2nd pass
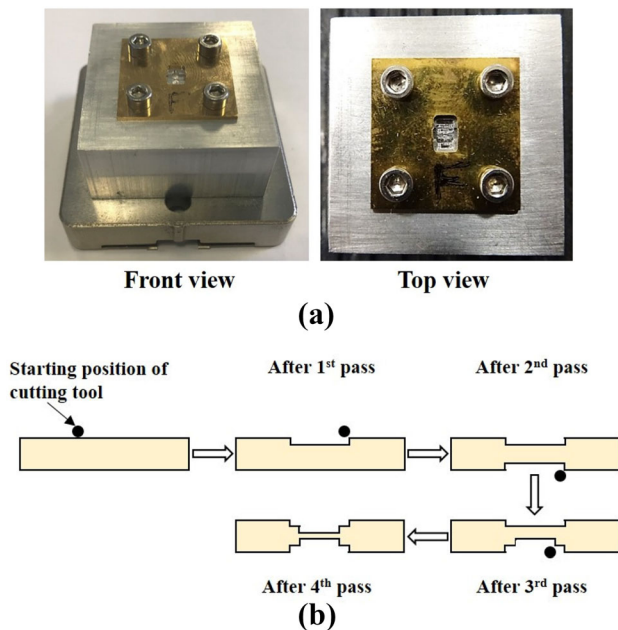
After 4th pass   After 3rd pass

(b)

Fig. 2. (a) Sample holder used to hold the material during machining, (b) Schematic representation of steps of material removal to obtain the sample.

thickness to 50 μm and 400 μm, respectively. Note that the thickness can be further reduced by polishing.

Dimensional Accuracy and Damage Characterization

The specimens were first observed under optical microscope to measure the dimensions and confirm no visible cracks/damages induced by micromilling. Figure 3a shows an example of specimens with aimed gauge widths of 75 μm and 500 μm. Minimum burrs were formed and no bending/buckling were observed in gauge sections. The dimensional accuracy was better than 99.5% on average as shown in Fig. 3b. Also surface roughness was measured for the machined surfaces. The common measure of surface roughness are Ra (average between peaks and valleys on the surface), Rz (average of consecutive highest peaks and lowest valleys) and Rq (root mean square average of height variation from the mean line). Random specimens were chosen and the non contact optical metrology estimated values of Ra, Rq and Rz are (0.17 $\pm$ 0.04) μm, (0.21 $\pm$ 0.06) μm and (1.19 $\pm$ 0.23) μm respectively. Such low values clearly indicate a smoother surface.

Typically, micromachining leads to rapid heating and quenching process on the surface, which results in ultrafine grain structure.[42] Subsurface damage induced by micromilling was characterized by quantifying the misorientation, fragmentation, and recrystallization of surface grains. Single crystal specimens were fabricated to characterize surface damage as shown in Fig. 4a, which depicts an EBSD scan of the surface from single crystal nickel specimen with milled edges. The damage layer is typically less than 2 μm as demonstrated by the Kernel Average Misorientation (KAM) measured along three lines shown in Fig. 4b. Careful polishing and subsequent electropolishing was performed for all specimens which effectively removed this layer without any noticeable impact on the bulk constitutive response of the tested specimens.

Mechanical Testing

We performed mechanical tests on mesoscale specimens using an Instron$^{\text{TM}}$ universal testing machine (UTM) Instron$^{\text{TM}}$ 5944, equipped with a 500 N load cell. Standard Instron wedge action grips were used to hold the samples during tensile load application. Given that the laser extensometer

Table I. Summary of the cutting parameters used to machine submillimetre gauge sections

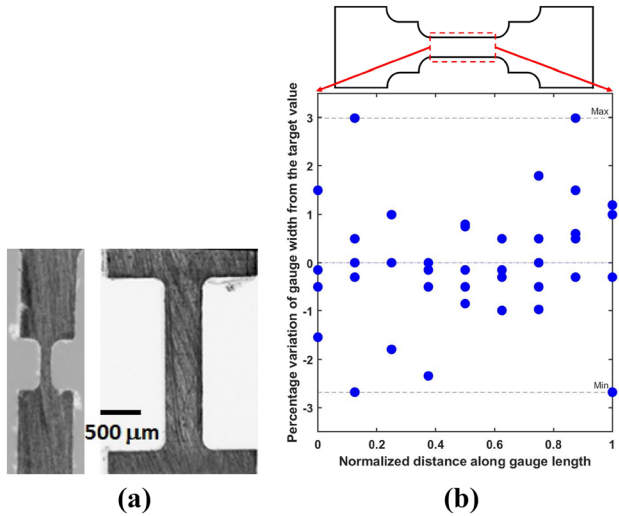| Process	Cutting tool type	Cutting speed	Feed rate	Depth of Cut
Making blanks	ϕ 1.5 mm carbide	3000 rpm	100 mm-min^{-1}	0.1 mm per pass
Specimen fabrication	ϕ 0.3 mm carbide	15000 rpm	200 mm-min^{-1}	0.1 mm per pass

(a)   **(b)**

Fig. 3. (a) Optical image of the fabricated specimens having 75 μm and 500 μm aimed gauge width respectively, (b) Dimensional accuracy of gauge width fabrication in percentage along the gauge length. Because of multiple sizes of specimens, gauge length was normalized.

integrated to the UTM can not resolve submillimeter samples, compliance correction was applied to the raw testing dataset following.[43] The raw displacement data in the elastic regime from experiments are sum of deformation of specimen and machine. This can be expressed as

$$h_{\exp} = F_{\exp}[(h_{\text{init,m}}/A_m E_m) + (h_{\text{init,s}}/A_s E_s)] \qquad (1)$$

where h and F represent displacement and load respectively, A is cross-section area and E is Young's modulus. Subscripts exp denotes raw data, init denotes initial values, m and s denote machine and specimen respectively. The only unknown is ($h_{\text{init,m}}/A_m E_m$) which was considered as the correction factor for machine compliance. Estimating this factors using raw data, compliance correction was applied to obtain specimen displacement only. Figure 5 shows as example of the correction to the obtained load–displacement data which was used further to calculate the stress–strain response.

RESULTS

Polycrystalline Specimens

We evaluated polycrystalline copper samples fabricated with gauge widths ranging from 75 μm to 3 mm and 500 μm thickness. The microstructure of a copper sample is shown in Fig. 6a. These specimens were deformed at a strain rate of 10^{-3} s^{-1} until reaching the maximum load as shown in Fig. 6b. The results demonstrate an evident size effect, in which a smaller gauge width resulted in a significant stress increase. A width of 500 μm and above behaves close to macroscopic behaviour and can be considered as the limit below which geometric size dominates the mechanical behaviour.
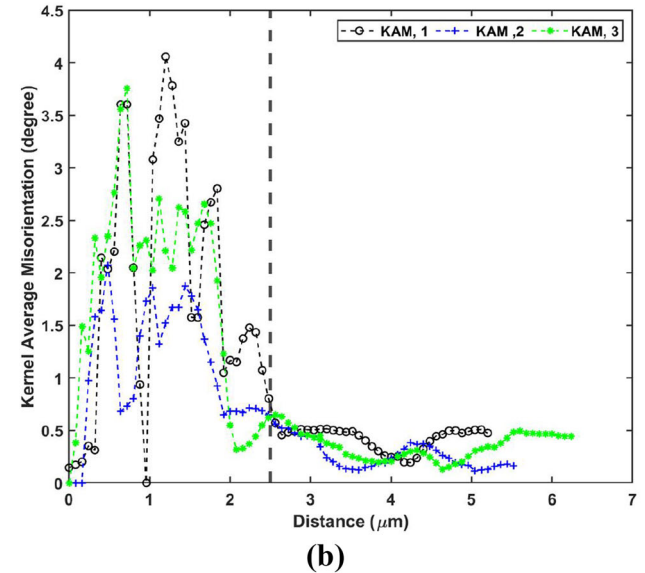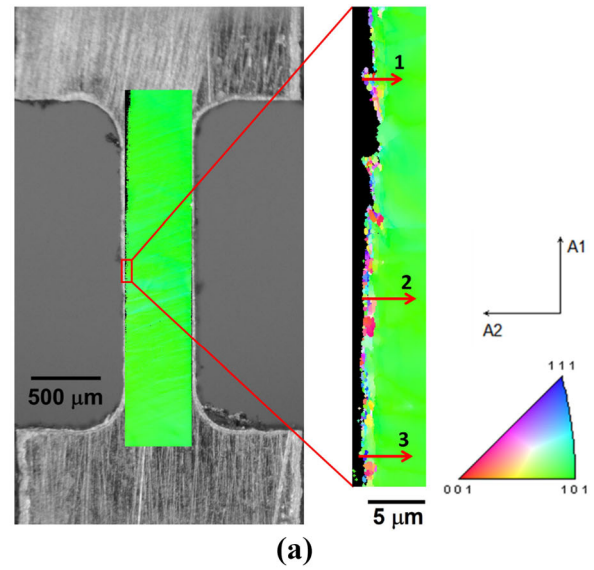

(a)

(b)

Fig. 4. (a) EBSD scan of a single crystal Ni specimen after machining. The color coding in figures is according to the standard triangle. (b) KAM line profile along the lines (as indicated by arrows in Fig 4a) revealing the extent of subsurface damaged layer. x = 0 indicates outer surface of specimen and the dotted vertical line shows maximum extent of damaged layer ($\sim$2.5 μm) (Color figure online).

Single Crystal Specimens

Next, high purity single crystal nickel ($>$ 99.999 wt% Ni) with (111) crystallographic orientation was cut into small coupons of 12 mm $\times$ 2 mm $\times$ 0.5 mm. Micro-tensile specimens with cross-sectional area of 100 μm $\times$ 500 μm or 500 μm $\times$ 500 (gauge width $\times$ thickness) and gauge length of 400 μm or 2000 μm respectively were fabricated as described earlier. Specimens were uniaxially deformed up to maximum load (or until a load drop was observed corresponding to appearance of necking in the specimen) at a crosshead displacement rate of 0.1 mm-min^{-1}.
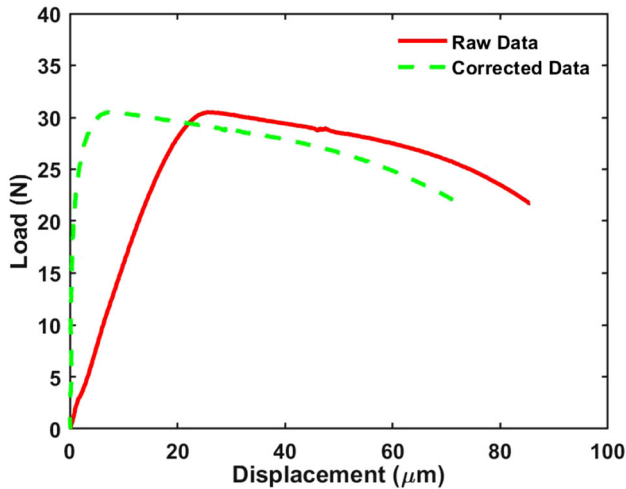
Fig. 5. Illustration of the compliance correction of the tested data using a nickel polycrystalline specimen.
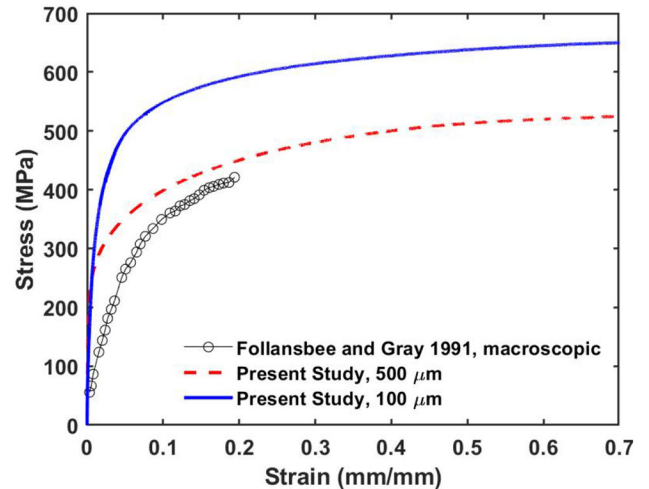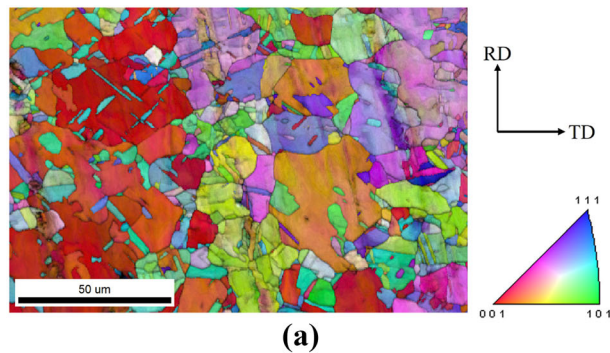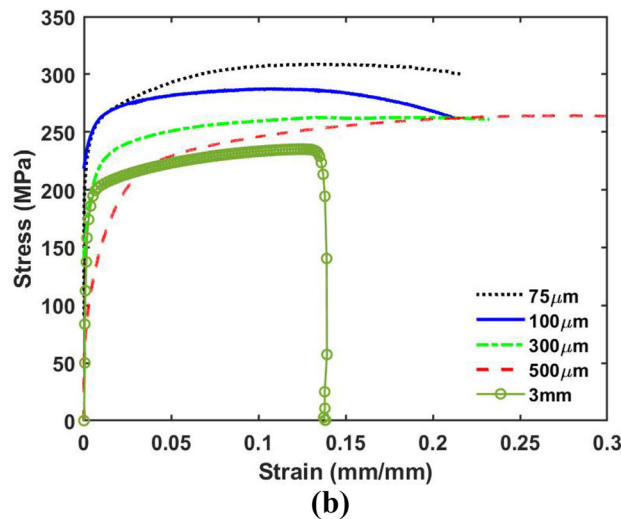

Fig. 7. Flow curve of single crystal Ni (111) orientation with two different gauge widths and thickness of 400 μm. For comparison with macroscopic deformation, results from Ref. 44 is included.

Fig. 6. (a) EBSD map of polycrystalline copper, (b) Flow curves of 500 μm thick polycrystalline copper with different gauge widths. A substandard size specimen (ASTM E8, substandard defined as macroscopic here) from the same material is included for comparison.

Figure 7 presents the stress–strain curves for different specimen sizes and demonstrates a similar effect of gauge width on stress as those shown in Fig. 6b. Multiple specimens of similar sizes were tested for polycrystalline or single crystals and the deformation response was similar. The results for the sample 500 μm in width agree with the macroscopic single crystal response reported in the literature.[44] Hence, Figs. 6b and 7 suggest that a gauge width of 500 μm can be regarded as a macroscopic sample, but notable size effects are apparent when the gauge is reduced to 100 μm. Interestingly, these results are in agreement with the lack of size effect for samples above ~250 μm by Keller and Hug,[45] but an effect from grain size around ~100 μm by Feaugas and Haddou.[46]

Single Crystal Specimens for Engineering Alloys

Production of single crystals is difficult for pure metals and near to be impossible for many engineering alloys. However, additive manufacturing parameters can be adjusted to engineer microstructures and development architectured structures.[47] Hence, we employed an additively manufactured process to produce large grains in Ni-20Cr alloy from which single crystal mesoscale specimens were machined. First, an EBSD scan was performed on the whole strip to identify grains of about 500 μm length and between 40 and 100 μm width. The grain(s) of interest (GoI) were marked by horizontal lines using FIB which are visible under optical microscope (Fig. 8a). Using these markers, specimens were fabricated with 40 μm × 460 μm (gauge width × thickness) and a gauge length of 200 μm. Deformation was carried out at a crosshead speed of 0.1 mm-min^{-1} till 10% deformation (shown in Fig. 8b). The results prove the capability of the developed method to extract single crystal specimens from alloys which is a challenging task and further reliable testing of the fabricated samples.
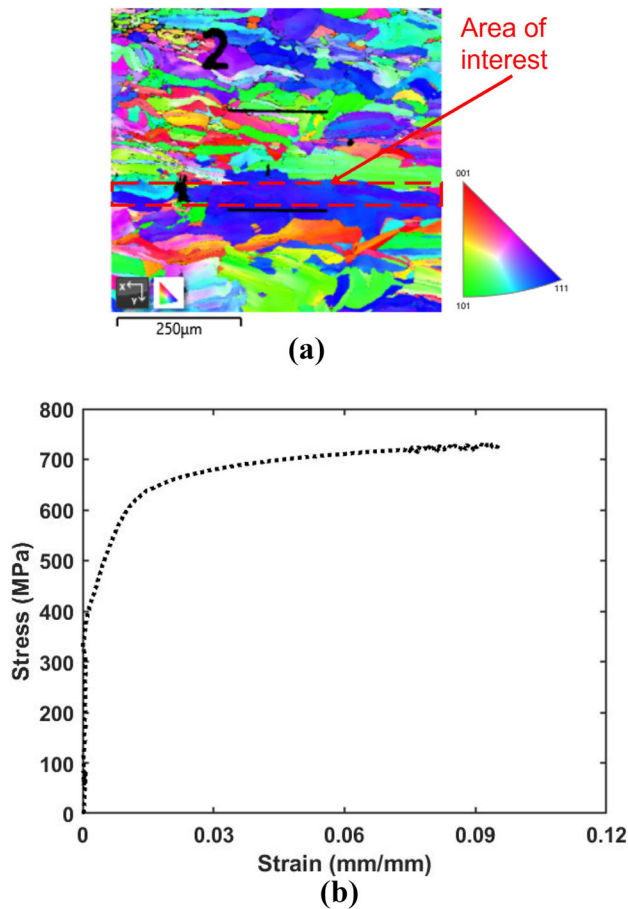
Fig. 8. (a) EBSD map of Ni-20Cr alloy with the interested grain marked by FIB, (b) Tensile deformation of a single crystal Ni-Cr alloy.

DISCUSSION AND CONCLUSION

This work presented a simple, high precision, and reliable specimen fabrication method for submillimetre mechanical specimens. We demonstrated a novel experimental protocol that can consistently assess the mechanical response of single crystals and polycrystals from numerous metals and engineering alloys. Notably, this approach was applied to additive manufacturing material to produce large grains and quantify the response of individual crystals. Hence, the proposed mesoscale testing approach can be combined with a number manufacturing routes (additive, heat treatments, electrodeposition) to produce large columnar grains in various metals e.g. titanium, stainless steels, nickel based alloys and aluminum alloys.[48]

Mesoscale tests can fill out a gap in experimental data for samples between 50 μm to 500 μm. Samples with these dimensions are valuable to characterize scarce material or to understand deformation mechanisms not directly observed at macro or micro scale testing. Hence, these experiments can result in important data to validate independently the physics described by constitutive models. In particular, our research has shown that,

- Micromachining can successfully fabricate specimens with gauge widths ranging from 75–500 μm with double notches to reduce the chances of buckling or bending. Specimens were fabricated for aluminium, nickel and copper, either pure or alloyed conditions, which demonstrates that the approach can work for a wide range of materials with appropriate cutting tools. Machining induced a plastically deformed layer less than 2 μm in thickness, which did not affect the constitutive response and was removed by electropolishing,
- A grain-specific fabrication method is designed as an extension to the developed method for obtaining single crystal specimens from alloyed materials which is limited in literature. The method is cheaper than producing single crystals through conventional ways and can be used for engineering alloys,
- A conventional UTM can perform the mechanical testing of these small specimens in contrast to in-situ testing with special grips or nanoindenter,
- Specimens with gauge width $\sim$500 μm seem to saturate size effects and closely approximate the macroscopic stress - strain response.

DATA AVAILABILITY

All data generated or analyzed during this study are included in this published article.

CONFLICT OF INTEREST

On behalf of all authors, the corresponding author states that there is no conflict of interest.

OPEN ACCESS

REFERENCES

1. S. Dindarlou, and G.M. Castelluccio, *Int. J. Plast* 155, 103306 (2022).
2. F. Ashraf, and G.M. Castelluccio, *Int. J. Plast* 161, 103494 (2023).
3. D. Kiener, W. Grosinger, G. Dehm, and R. Pippan, *Acta Mater.* 56(3), 580–592 (2008).
4. Gong, J., Benjamin Britton, T., Cuddihy, M.A., Dunne, F.P.E., Wilkinson, A.J.: Acta Materialia 96, 249–257 (2015).
5. A.D. Smith, J. Donoghue, A. Garner, B. Winiarski, E. Bousser, J. Carr, J. Behnsen, T. Burnett, R. Wheeler, K. Wilford, P.J. Withers, and M. Preuss, *Exp. Mech.* 59(8), 1113–1125 (2019).
6. ASTM E8/E8M standard test methods for tension testing of metallic materials (2010).
7. G.B. Rathmayr, A. Bachmaier, and R. Pippan, *J. Test. Eval.* 41(4), 635–646 (2013).
8. R. Klueh, *Fusion* 2(3), 407–416 (1985).
9. H. Vo, A. Reichardt, D. Frazer, N. Bailey, P. Chou, and P. Hosemann, *J. Nucl. Mater.* 493, 336–342 (2017).
10. P. Hosemann, *Scripta Mater.* 143, 161–168 (2018).
11. A. Barnoush, P. Hosemann, J. Molina-Aldareguia, and J.M. Wheeler, *MRS Bull.* 44(6), 471–477 (2019).
12. G.M. Castelluccio, A.A. Yawny, J.E. Perez Ipiña, and H.A. Ernst, *Strain* 48(1), 68–74 (2011).
13. G.M. Castelluccio, J.E. Perez Ipiña, A.A. Yawny, and H.A. Ernst, *Eng. Fract. Mech.* 98, 52–63 (2013).
14. Y. Kihara, T. Nagoshi, T.-F.M. Chang, H. Hosoda, S. Tatsuo, and M. Sone, *Mater. Lett.* 153, 36–39 (2015).
15. K. Ng, and A. Ngan, *Philos. Mag. Lett.* 87(12), 967–977 (2007).
16. L. Farbaniec, H. Couque, and G. Dirras, *Int. J. Eng. Sci.* 119, 192–204 (2017).
17. D. Casari, L. Pethö, P. Schürch, X. Maeder, L. Philippe, J. Michler, P. Zysset, and J. Schwiedrzik, *J. Mater. Res.* 34(14), 2517–2534 (2019).
18. D.M. Dimiduk, M.D. Uchic, and T.A. Parthasarathy, *Acta Mater.* 53(15), 4065–4077 (2005).
19. C.P. Frick, S. Orso, and E. Arzt, *Acta Mater.* 55(11), 3845–3855 (2007).
20. D. Kiener, C. Motz, and G. Dehm, *J. Mater. Sci.* 43(7), 2503–2506 (2008).
21. M. Asadipoor, A.P. Anaraki, J. Kadkhodapour, S. Sharifi, and A. Barnoush, *Mater. Sci. Eng., A* 772, 138762 (2020).
22. M. Camara, J.C. Rubio, A. Abrão, and J. Davim, *J. Mater. Sci. Technol.* 28(8), 673–685 (2012).
23. K. Ahmmed, C. Grambow, and A.-M. Kietzig, *Micromachines* 5(4), 1219–1253 (2014).
24. Y. Natarajan, P.K. Murugesan, M. Mohan, and S.A.L.A. Khan, *J. Manuf. Process.* 49, 271–322 (2020).
25. M. Phaneuf, *Micron* 30(3), 277–288 (1999).
26. C.A. Volkert, and A.M. Minor, *MRS Bull.* 32(5), 389–399 (2007).
27. N. Bassim, K. Scott, and L.A. Giannuzzi, *MRS Bull.* 39(4), 317–325 (2014).
28. D. Kiener, C. Motz, M. Rester, M. Jenko, and G. Dehm, *Mater. Sci. Eng., A* 459(1–2), 262–272 (2007).
29. A. Revelly, G. Monpara, I. Samajdar, K.M. Krishna, R. Tewari, D. Srivastava, G. Dey, and A. Panwar, *J. Nucl. Mater.* 467, 155–164 (2015).
30. J. Fleischer, T. Masuzawa, J. Schmidt, and M. Knoll, *J. Mater. Process. Technol.* 149(1–3), 246–249 (2004).
31. K. Liu, B. Lauwers, and D. Reynaerts, *Int. J. Adv. Manuf. Technol.* 47(1–4), 11–19 (2010).
32. S. Mishra, and V. Yadava, *Opt. Lasers Eng.* 73, 89–122 (2015).
33. M.J. Pfeifenberger, M. Mangang, S. Wurster, J. Reiser, A. Hohenwarter, W. Pfleging, D. Kiener, and R. Pippan, *Mater. Des.* 121, 109–118 (2017).
34. Q. McCulloch, J. Gigax, and P. Hosemann, *JOM* 72(4), 1694–1702 (2020).
35. M.P. Echlin, A. Mottura, C.J. Torbet, and T.M. Pollock, *Rev. Sci. Instrum.* 83(2), 023701 (2012).
36. S.J. Randolph, J. Filevich, A. Botman, R. Gannon, C. Rue, and M. Straw, *J. Vac. Sci. Technol., B: Nanotechnol. Microelectron.: Mater., Process., Meas., Phenom.* 36(6), 06–11 (2018).
37. D. Pan, M. Chen, P. Wright, and K. Hemker, *Acta Mater.* 51(8), 2205–2217 (2003).
38. M.Z. Alam, S. Kamat, V. Jayaram, and D.K. Das, *Acta Mater.* 61(4), 1093–1105 (2013).
39. D. Texier, D. Monceau, J.-C. Salabura, R. Mainguy, and E. Andrieu, *Mater. High Temp.* 33(4–5), 325–337 (2016).
40. B. Bhattacharyya, S. Mitra, and A. Boro, *Robot. Comput.-Integr. Manuf.* 18(3–4), 283–289 (2002).
41. D.J. Guckenberger, T.E. de Groot, A.M. Wan, D.J. Beebe, and E.W. Young, *Lab. Chip* 15(11), 2364–2378 (2015).
42. Z. Pan, Y. Feng, and S.Y. Liang, *Manuf. Rev.* 4, 5 (2017).
43. N.I. Rohaizat, K. Alharbi, C. Pinna, H. Ghadbeigi, D.N. Hanlon, and I.A. Azid, Using a Correction Factor to Remove Machine Compliance in a Tensile Test on DP1000 Steel Validated with 2D Digital Image Correlation Technique, in *Progress in Engineering Technology III*. ed. by M.H. Abu Bakar, M. Nurhidayat Zahelem, and A. Öchsner (Springer, Cham, 2021), pp. 113–123.
44. P. Follansbee, and G. Gray, *Int. J. Plast.* 7(7), 651–660 (1991).
45. C. Keller, and E. Hug, *Int. J. Plast.* 98, 106–122 (2017).
46. X. Feaugas, and H. Haddou, *Metall. Mater. Trans. A.* 34(10), 2329–2340 (2003).
47. J. Pistor, and C. Körner, *Sci. Rep.* 11(1), 1–8 (2021).
48. T. DebRoy, H. Wei, J. Zuback, T. Mukherjee, J. Elmer, J. Milewski, A.M. Beese, A.D. Wilson-Heid, A. De, and W. Zhang, *Progr. Mater. Sci.* 92, 112–224 (2018).